

Complex Exponential Signal Recovery with Deep Hankel Matrix Factorization

Yihui Huang[†], Jinkui Zhao[†], Zi Wang, Di Guo, Xiaobo Qu^{*}

Abstract—Exponential is a basic signal form and how to fast acquire these signals is one of the fundamental problems and frontiers in signal processing. To achieve this goal, partial data may be acquired but result in the serious artifacts in its spectrum, which is the Fourier transform of exponentials. Thus, reliable spectrum reconstruction is highly expected in the fast sampling in many applications, such as chemistry, biology, and medical imaging. In this work, we propose a deep learning method whose neural network structure is designed by unrolling the iterative process in the model-based state-of-the-art exponentials reconstruction method with low rank Hankel matrix factorization. With the experiments on synthetic and realistic biological signals, we demonstrate that the new method yields much lower reconstruction errors and more accuracy in spectrum parameter quantification than another state-of-the-art deep learning method, while costs much less time than the model-based reconstruction methods.

Index Terms—exponential signal, deep learning, Hankel matrix completion, low rank, matrix factorization

I. INTRODUCTION

EXPONENTIAL function is basic and very important in signal processing. In many practical applications, signals can be approximated by the superposition of a few numbers of complex exponential functions. Examples include antenna signals in telecommunication [1-3], images in fluorescence microscopy [4], analog-to-digital conversion in electronic systems [5], signals function in the theory of finite rate of

innovation [6], and time-domain signals in Nuclear Magnetic Resonance (NMR) spectroscopy [7-12]. Thus, achieving high-quality recovery of the exponential signals has great significance in many fields. The corresponding signal in these applications can be represented as follows:

$$x(t) = \sum_{r=1}^R (A_r e^{2\pi i f_r + i\phi_r}) e^{-\frac{t}{\tau_r}}, \quad (1)$$

where $f_r \in [0, 1)$ is the normalized frequency, $\phi_r \in [0, 2\pi)$ is the phase, $A_r \in \mathbb{C}$ is the amplitude, $\tau_r \in \mathbb{R}_+$ is the damping factor, R is the number of exponentials, and $r = 1, \dots, R$. For instance, in biological NMR spectroscopy, $x(t)$ is a sum of damped complex sinusoids that characterizes the acquired time-domain signal [7].

Due to all kinds of objective restrictions such as hardware limitations and high experimental costs, it is hard to fully sample the signal in many circumstances. Take NMR spectroscopy as an example, Non-Uniform Sampling (NUS) is widely used to accelerate the data acquisition [7, 13-18]. Let

$\mathbf{x} = [x(1), \dots, x(n)]^T \in \mathbb{C}^n$ be the non-uniform sampled signal.

In this paper, we aim to recover the signal \mathbf{x} from the partial measured $\mathbf{y} \in \mathbb{C}^m$ ($m < n$).

In the past two decades, several methods have been raised to exploit the sparsity of \mathbf{x} in the frequency domain. At first, utilizing the sparsity of \mathbf{x} with the discrete frequencies, the signal can be recovered from a small number of samples using conventional compressed sensing [19]. However, given that true frequencies always take continuous values, total variation or atomic norm minimization method [20] were presented by exploiting the sparsity of \mathbf{x} with the continuous-valued frequencies. Other methods using spectral line-shape estimation [21] and tensor structures [22] are also suggested.

Recently, researchers used the low rank property of the Hankel matrix formed by the exponential signal \mathbf{x} [23-28], turning the signal recovery problem into a Low Rank Hankel Matrix Completion (LRHMC) problem. Since the minimization problem of the rank was NP-hard, some approaches utilized the nuclear norm to relax it into a convex optimization one [25, 26, 29]. These approaches showed great potential in the LRHMC problem due to its high acceleration rate and fidelity. However, to minimize the nuclear norm, Singular Value Thresholding (SVT) [30] was introduced in

This work was supported in part by the National Natural Science Foundation of China (NSFC) under grants 61971361, 61871341 and U1632274, the National Key R&D Program of China under grant 2017YFC0108703, the Natural Science Foundation of Fujian Province of China under grant 2018J06018, the Fundamental Research Funds for the Central Universities under grant 20720180056, and Xiamen University Nanqiang Outstanding Talents Program. And the authors thank to INVIDA for donating the GPU. ([†]Equal Contributions, ^{*} Corresponding author)

Yihui Huang, Jinkui Zhao, Zi Wang, and Xiaobo Qu are with the Department of Electronic Science, Fujian Provincial Key Laboratory of Plasma and Magnetic Resonance, Xiamen University, Xiamen, China (e-mail: quxiaobo@xmu.edu.cn).

Di Guo is with the School of Computer and Information Engineering, Xiamen University of Technology, Xiamen, China.

some of the iterative methods, which usually took hours on Singular Value Decomposition (SVD) operation [7]. Although SVD-Free method [9, 11, 31] was raised to reduce the computational time of each iteration, the overall cost of time still needed to be further improved due to the large number of iterations in the conventional optimization algorithm.

So far, many applications have met with the problem of the high computational complexity of exponential signal recovery, including signal retrieval of antenna and radar [1, 2, 32], signal recovery in ultra-wideband [33, 34], and high-resolution signal reconstruction in NMR spectroscopy [7, 35, 36]. It means that the rapid recovery of high-quality exponential signals is widely required and is a huge challenge.

Inspired by the great achievement of deep learning (DL) [37-39], DL-based methods have been introduced into biological NMR spectroscopy [36, 40] and have shown great potential in accelerating the reconstruction process and achieving high-quality reconstruction performances [40]. DL methods are a kind of data-driven method, which require a large training set. These DL methods successfully trained the neural network using solely synthetic NMR data with the exponential function, which solved the critical problem in NMR spectroscopy that a large amount of realistic data was not easy to be acquired to constitute the training set. Nevertheless, like a black-box, DL methods have long been criticized for its lack of interpretability, and it is difficult to understand what the network had learned while implementing various mappings.

In this work, we propose a new network architecture to recover complex exponential signals by unfolding the established iteration model. Our design of architecture starts from constraining the low rank property of the Hankel matrix which is arranged from exponential signals, and adopts matrix factorization measurement from the SVD-Free-based LRHMC method [9, 11, 31], to reconstruct undersampled signals. We unfold the iterative method to a fixed-length deep neural network, called Deep Hankel Matrix Factorization network (DHMF). Given the success of training neural networks using solely synthetic data [40], we also generate a big dataset consists of synthetic data to drive our network to learn the appropriate mapping and internal parameters. Results on synthetic data demonstrate that, compared with the state-of-the-art methods, iterative Hankel matrix completion methods and deep learning methods, DHMF is much faster to recovery signals than the former one, and it is easier to be interpreted than the latter since it is rooted from the established reconstruction method. Moreover, the proposed method can surpass both of them in terms of robustness and reconstruction quality under some circumstances.

The rest of this paper is organized as follows. Section II introduces notations. In Section III, we introduce the mathematic formulation of Low Rank Hankel Matrix Factorization (LRHMF) approach [11], which is the iteration method we base on. In Section IV, we propose DHMF and its enhanced version, followed by the loss function and hyper-parameters of our network. Section V first elaborates on the scheme of generating the data set and training the network, then evaluates the recovery performance of the proposed DHMF on

synthetic data and realistic biological NMR data. At the end of the paper, we extend discussions on proposed DHMF in Section VI and Section VII finally concludes this work and gives an outlook of the future directions.

II. NOTATIONS

We start with the notation used throughout this paper. x represents a scalar, \mathbf{x} a vector, \mathbf{X} a matrix, \mathbf{I} an identity matrix. The j -th entry of a vector is denoted by \mathbf{x}_j and the (i, j) -th entry of a matrix is denoted by \mathbf{X}_{ij} . The notation $\|\cdot\|_p$ is the standard p -norm, $\|\cdot\|_*$ is the nuclear norm, and $\|\cdot\|_F$ represents the Frobenius norm. The transpose of vectors and matrices are denoted by \mathbf{x}^T and \mathbf{X}^T , while their conjugate transpose is denoted by \mathbf{x}^H and \mathbf{X}^H . \mathbf{X}^{-1} represents the inverse of the matrix \mathbf{X} . Superscript k denotes the number of iterations.

Operators are denoted by calligraphic letters. \mathcal{R} denotes the Hankel operator mapping the vector $\mathbf{x} \in \mathbb{C}^n$ to a Hankel matrix $\mathcal{R}\mathbf{x} \in \mathbb{C}^{n_1 \times n_2}$ with $n_1 + n_2 = n + 1$ as follows:

$$\mathcal{R}: \mathbf{x} \in \mathbb{C}^{n_1+n_2-1} \mapsto \mathbf{X} \in \mathbb{C}^{n_1 \times n_2}, \mathbf{X}_{ij} = \mathbf{x}_{i+j-1}, \quad (2)$$

and the corresponding inverse operator \mathcal{R}^* which turns a Hankel matrix to a vector is given by

$$\mathcal{R}^*: \mathbf{X} \in \mathbb{C}^{n_1 \times n_2} \mapsto \mathbf{x} \in \mathbb{C}^{n_1+n_2-1}, \mathbf{x}_g = \sum_{i+j-1=g} \frac{\mathbf{X}_{ij}}{(\mathcal{R}\mathbf{o})_{ij}}, \quad (3)$$

where $\mathbf{o} \in \mathbb{C}^{n_1+n_2-1}$ is the vector whose elements are all 1. For any $i \in \{1, \dots, n_1\}$ and $j \in \{1, \dots, n_2\}$.

III. RELATED WORK

In this section, we introduce the mathematic formulation of LRHMF method [11], which is an iterative optimization algorithm we base on.

Let vector $\mathbf{x} \in \mathbb{C}^n$ be a superposition of exponential functions. It has been proven that the rank of the Hankel matrix is equal to the number of exponentials in \mathbf{x} . LRHMC problem is to solve the reconstruction problem by utilizing the low rank property of the Hankel matrix as a constraint according to

$$\min_{\mathbf{x}} \|\mathcal{R}\mathbf{x}\|_* + \frac{\lambda}{2} \|\mathbf{y} - \mathbf{U}\mathbf{x}\|_2^2. \quad (4)$$

where \mathbf{x} is the signal we want to recover from the under-sampled data \mathbf{y} , \mathbf{U} denotes the under-sampled matrix. The first nuclear norm term is considered to be an indicator of the matrix rank, while the second term measures the data consistency. Regularization parameter λ tradeoffs between the low rankness and data consistency. Given a matrix \mathbf{X} , it has been shown that the following relationship holds true [41, 42]:

$$\|\mathbf{X}\|_* = \min_{\mathbf{P}, \mathbf{Q}} \frac{1}{2} (\|\mathbf{P}\|_F^2 + \|\mathbf{Q}\|_F^2), \text{ s.t. } \mathbf{P}\mathbf{Q}^H = \mathbf{X}. \quad (5)$$

To avoid SVD operation which is typically required when dealing with nuclear norm minimization, LRHMF use a factorized representation s.t. $\mathcal{R}\mathbf{x} = \mathbf{P}\mathbf{Q}^H$, where \mathbf{P} , \mathbf{Q} are

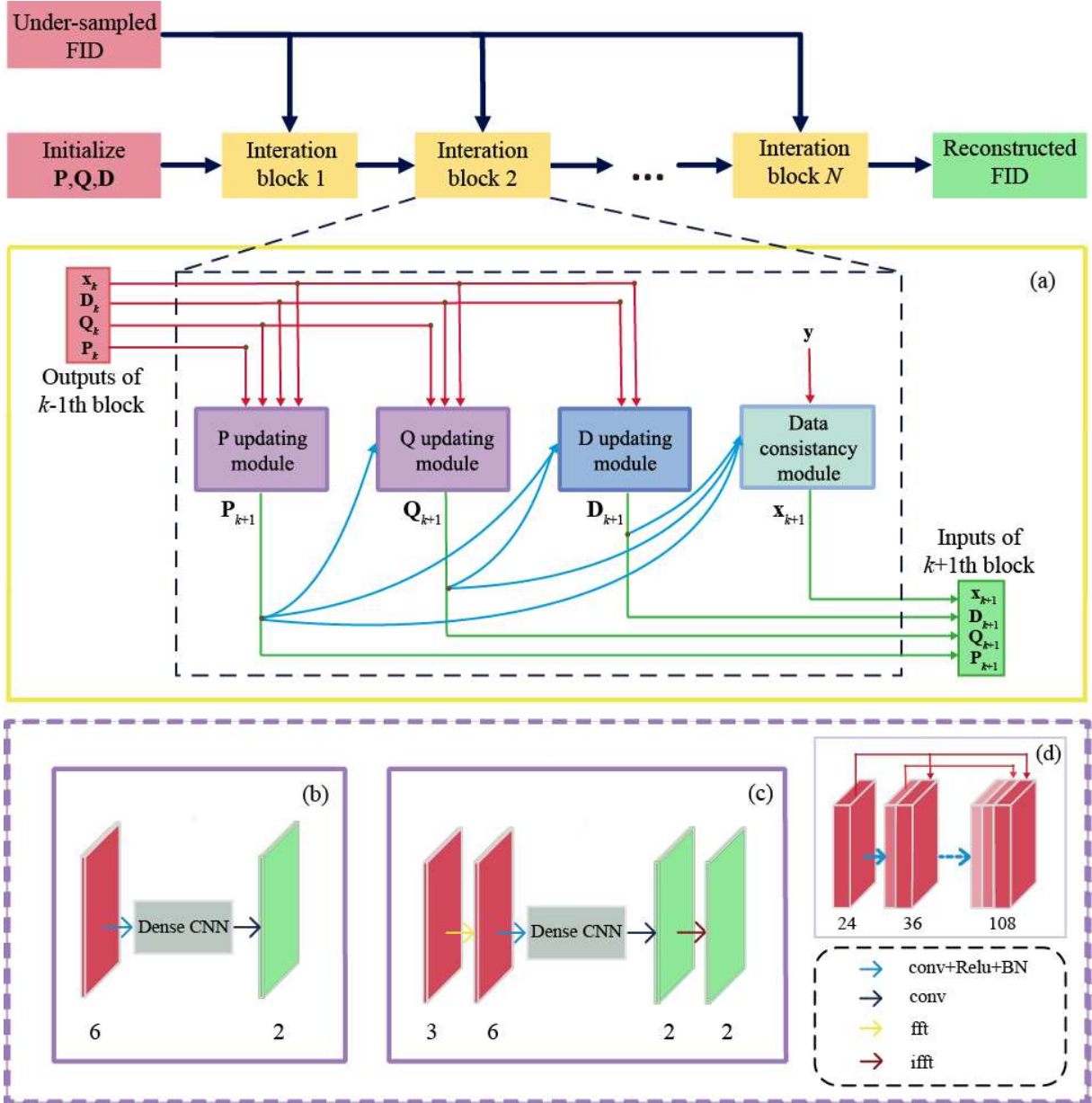


Fig. 1. The detailed architectures of DHMF. (a) Architecture of the k -th block in DHMF (panel), detailed structures of \mathbf{P} , \mathbf{Q} updating modules in DHMF (b) and in enhanced DHMF (c), (d) structure of dense convolutional network.

matrices with size $n_1 \times \tilde{r}$ and $n_2 \times \tilde{r}$. With this theorem, the nuclear norm minimization problem in (4) can be rewritten as:

$$\min_{\mathbf{x}, \mathbf{P}, \mathbf{Q}} \frac{1}{2} (\|\mathbf{P}\|_F^2 + \|\mathbf{Q}\|_F^2) + \frac{\lambda}{2} \|\mathbf{y} - \mathbf{U}\mathbf{x}\|_2^2, \text{ s.t. } \mathcal{R}\mathbf{x} = \mathbf{P}\mathbf{Q}^H. \quad (6)$$

Alternating Direction Method of Multipliers (ADMM) is then introduced to solve this non-convex problem [7]. The augmented Lagrangian function of (6) is

$$L(\mathbf{x}, \mathbf{P}, \mathbf{Q}, \mathbf{D}) = \frac{1}{2} \|\mathbf{P}\|_F^2 + \frac{1}{2} \|\mathbf{Q}\|_F^2 + \frac{\lambda}{2} \|\mathbf{y} - \mathbf{U}\mathbf{x}\|_2^2 + \langle \mathbf{D}, \mathcal{R}\mathbf{x} - \mathbf{P}\mathbf{Q}^H \rangle + \frac{\beta}{2} \|\mathcal{R}\mathbf{x} - \mathbf{P}\mathbf{Q}^H\|_F^2 \quad (7)$$

where \mathbf{D} denotes the augmented Lagrange multiplier, $\langle \cdot, \cdot \rangle$ represents an inner product operator, parameters $\lambda > 0$, and

$\gamma > 0$ is used to balance between each term. By minimizing Eq. (7), the k -th iteration of the solution to (6) can be written as:

$$\begin{cases} \mathbf{x}^{k+1} = (\lambda \mathbf{U}^T \mathbf{U} + \gamma \mathcal{R}^* \mathcal{R})^{-1} (\lambda \mathbf{U}^T \mathbf{y} + \gamma \mathcal{R}^* (\mathbf{P}^k (\mathbf{Q}^k)^H - \mathbf{D}^k)) \\ \mathbf{P}^{k+1} = \gamma (\mathcal{R} \mathbf{x}^{k+1} + \mathbf{D}^k) \mathbf{Q}^k (\gamma (\mathbf{Q}^k)^H \mathbf{Q}^k + \mathbf{I})^{-1} \\ \mathbf{Q}^{k+1} = \gamma (\mathcal{R} \mathbf{x}^{k+1} + \mathbf{D}^k)^H \mathbf{P}^{k+1} (\gamma (\mathbf{P}^{k+1})^H \mathbf{P}^{k+1} + \mathbf{I})^{-1} \\ \mathbf{D}^{k+1} = \mathbf{D}^k + \tau^k (\mathcal{R} \mathbf{x}^{k+1} - \mathbf{P}^{k+1} (\mathbf{Q}^{k+1})^H) \end{cases}, \quad (8)$$

where τ is the footstep of one iteration. As an iterative algorithm, the optimization process still requires lengthy computational time. Moreover, with the reduction of sampling rate and the increasing of the length of each dimension, it requires much more iterations to achieve high-quality reconstruction performance, resulting in a non-fixed

reconstruction complexity. Although the natural idea is to introduce DL to optimize (4), directly using SVD operation in the network may result in the failure of convergence [43]. Here, we develop a Deep Hankel Matrix Factorization network (DHMF) based on the LRHMF, whose architecture is shown in Fig. 1.

IV. PROPOSED METHOD

In this section, we propose DHMF to unfold the iterative method, LRHMF [11]. We first introduce the basic DHMF and explain how each module is designed. We then propose the enhanced DHMF. Finally, we show the loss function and hyper-parameters of our DHMF.

A. Deep Hankel Matrix Factorization Network Structure

Compared with traditional iterative methods, DL has shown great potential in accelerating the reconstruction process, but is lack of interpretability at present. We consider to design a deep learning network called DHMF by unfolding the LRHMF [11] to make the network structure easier to be interpreted. Matrix multiplications in (8) are replaced by convolutional layers and, therefore, a single block of DHMF can be correspondingly designed as four parts: \mathbf{P} updating module and \mathbf{Q} updating module used to update the factorized matrix \mathbf{P} and \mathbf{Q} , \mathbf{D} updating module for updating the auxiliary matrix \mathbf{D} , and data consistency modules used to restore reconstructed signal \mathbf{x} . Thus, the total DHMF turns out to be a stack of blocks with the number of K . A diagram for a single network block is shown in Fig. 1.

1) Updating module of \mathbf{P} and \mathbf{Q}

Here, we use convolution operations to map the inverse operations as well as their relationship between other variables approximately during the update of matrix \mathbf{P} and \mathbf{Q} . The equations for k -th ($k = 1, 2, \dots, K$) \mathbf{P} , \mathbf{Q} updating modules are obtained as:

$$\begin{aligned} \mathbf{P}^{k+1} &= \mathcal{P}^k((\mathcal{R}\mathbf{x}^k + \mathbf{D}^k)\mathbf{Q}^k, \mathbf{Q}^k, \mathbf{P}^k) \\ \mathbf{Q}^{k+1} &= \mathcal{Q}^k((\mathcal{R}\mathbf{x}^{k+1} + \mathbf{D}^k)^H \mathbf{P}^{k+1}, \mathbf{P}^{k+1}, \mathbf{Q}^k) \end{aligned} \quad (9)$$

where convolution operators \mathcal{P} , \mathcal{Q} are trained by the network. We choose dense convolutional network to learn the mapping because it can maintain maximum information through the data flow [44]. Rectified linear unit (ReLU) is chosen as the activation function and batch normalization (BN) is also used between convolution layers to accelerate convergence speed. Meanwhile, in the updating module of \mathbf{P}^{k+1} or \mathbf{Q}^{k+1} , variable \mathbf{P}^k or \mathbf{Q}^k is also provided to obtain maximum convolution features. Real parts and imaginary parts of the input of each updating module are concatenated together while entering the sub-network, and the output of each module also has two channels. By applying SVD, the initial value of \mathbf{P} and \mathbf{Q} are provided from the left and right singular vector of the undersampled data, respectively.

2) Updating module of \mathbf{D}

For \mathbf{D} updating module, the module is calculated by:

$$\mathbf{D}^{k+1} = \mathbf{D}^k + \tau(\mathcal{R}\mathbf{x}^{k+1} - \mathbf{P}^{k+1}(\mathbf{Q}^{k+1})^H), \quad (10)$$

and we set the footsteps parameter τ as a constant and initialize \mathbf{D} by zero matrix in the first block.

3) Data consistency module

Since the update of \mathbf{x} has an explicit practical significance that the reconstruction data shall be aligned to acquired data [45], we propose the data consistency module, and the k -th data consistency module can be represented as:

$$\mathbf{x}^{k+1} = \mathcal{S}(\mathbf{y}, \mathcal{R}^*(\mathbf{P}^{k+1}(\mathbf{Q}^{k+1})^H - \mathbf{D}^{k+1})), \quad (11)$$

where \mathcal{S} denotes the data consistency operator. Let $\hat{\mathbf{x}}^{k+1}$ be the restored data obtained by $\mathcal{R}^*(\mathbf{P}^{k+1}(\mathbf{Q}^{k+1})^H - \mathbf{D}^{k+1})$, (11) is equal to the following relationship:

$$\mathbf{x}_n^{k+1} = \begin{cases} \hat{\mathbf{x}}_n^{k+1} & , \text{ if } n \notin \mathbf{U} \\ \frac{\hat{\mathbf{x}}_n^{k+1} + \lambda \mathbf{y}}{1 + \lambda} & , \text{ if } n \in \mathbf{U} \end{cases}, \quad (12)$$

where \mathbf{U} is the set of positions for sampled exponential signal, n is the index of the signal. Equation (12) implies that the exponential signal at the location of sampled data points should be balanced between the acquired data points in the initial data \mathbf{y} and the predicted data point $\hat{\mathbf{x}}_n^{k+1}$ which obtained by network with the balance parameter λ .

We conduct an experiment with noise-free training datasets and a toy example consists of five peaks, to demonstrate the necessity of the data consistency module. As is shown in Fig. 2, the spectrum artifacts are firstly removed to some degree by \mathbf{P} and \mathbf{Q} updating blocks in their respective domain. By

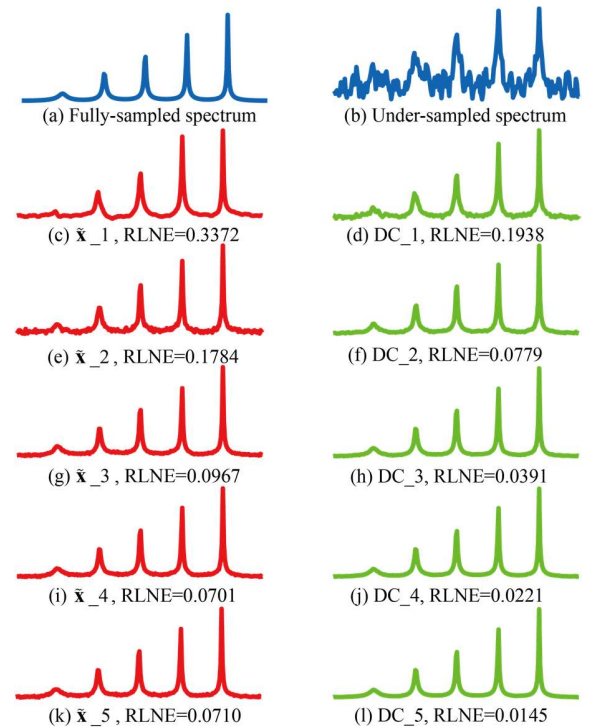


Fig. 2. The illustrative results before and after the data consistency in frequency domain. Note: $\hat{\mathbf{x}}$, DC, and the number (1,2,3,4,5) denote the outputs before and after the data consistency, and the order of reconstruction stage, respectively. The final output of the network is (l) DC-5.

calculating $\tilde{\mathbf{x}} = \mathcal{R}^*(\mathbf{P}\mathbf{Q}^H - \mathbf{D})$, we get the preliminary reconstructed spectrum $\tilde{\mathbf{x}}$ (Figs. 2-(c)(e)(g)(i)(k)). The spectrum quality is then enhanced by utilizing data consistency (Fig. 2-(d)(f)(h)(j)(l)) and further improvement is acquired by repeating the designed block several times. As a quantitative criteria, the relative least normalized error (RLNE) is defined as:

$$\text{RLNE} = \frac{\|\mathbf{x} - \tilde{\mathbf{x}}\|_2}{\|\mathbf{x}\|_2}, \quad (13)$$

where \mathbf{x} is the fully sampled spectrum and $\tilde{\mathbf{x}}$ is the reconstructed spectrum. The lower RLNE represents for the higher consistency between \mathbf{x} and $\tilde{\mathbf{x}}$. Here, RLNE between $\tilde{\mathbf{x}}$ and labels, the outputs of the data consistency and labels in different blocks are shown in Fig.2, which demonstrates our illustration numerically.

B. Enhanced Deep Hankel Matrix Factorization Network

Here, we propose enhanced DHMF to improve the reconstruction performance.

Considering that the previous DL method [40] which applies convolution operation in frequency domain for exponential signal reconstruction, we also change the convolution scope from time domain to frequency domain. Fig. 1(c) shows that compare with DHMF, fast Fourier transform (FFT) and inverse fast Fourier transform (iFFT) are added to inputs and outputs of \mathbf{P} and \mathbf{Q} updating module in the enhanced version, respectively. For matrixes \mathbf{P} , \mathbf{Q} with size $n_1 \times r$ and $n_2 \times r$, 1D-FFT and 1D-iFFT are applied in their first dimensions which have size n_1 and n_2 .

An experiment with noise-free training datasets is then conducted to show the performance, testing data is noise-free and consists of five peaks. Size r is chosen as 20. Fig. 3 shows

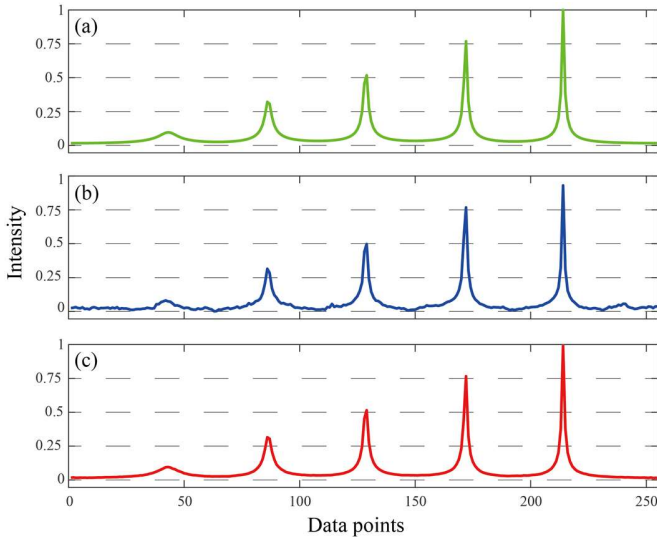


Fig. 3. Reconstructed synthetic signals of DHMF and enhanced DHMF in frequency domain, (a) is the fully sampled signal, (b) and (c) are the reconstructed by DHMF and enhanced DHMF, respectively. Compared with fully sampled signal, RLNE of reconstruction results is 0.1813 in DHMF, and is 0.0145 in enhanced DHMF.

that the signal restored by the enhanced DHMF obtains higher reconstruction quality on weak peaks, while DHMF introduced some artifacts.

C. Loss Function and Hyper-parameters

The loss function is chosen as the sum of the mean squared errors (MSE) between reconstructed signal $\hat{\mathbf{x}}_q$ and fully sampled signal \mathbf{s}_q . Let $\hat{\mathbf{P}}_q$ and $\hat{\mathbf{Q}}_q$ denote the output of \mathbf{P} updating module and \mathbf{Q} updating module, a typical solution of (8) is $\hat{\mathbf{P}}_q(\hat{\mathbf{Q}}_q)^H$, which is approximate to $\mathcal{R}\mathbf{s}_q$. Thus, we add the square of the Frobenius norm of matrices $(\hat{\mathbf{P}}_q(\hat{\mathbf{Q}}_q)^H - \mathcal{R}\mathbf{s}_q)$ in the loss function as the regularization term to guide the output. Since the output of each block possesses the same significance and size, differences between labels and the output of each block are added into loss function to achieve better results. The overall loss function in our implementation is

$$\mathcal{L}(\Theta) = \frac{1}{Q} \sum_{q=1}^Q \sum_{k=1}^K (\|\hat{\mathbf{x}}_q^k(\Theta^k) - \mathbf{s}_q\|_2^2 + \gamma \|\hat{\mathbf{P}}_q^k(\Theta^k) \hat{\mathbf{Q}}_q^k(\Theta^k)^H - \mathcal{R}\mathbf{s}_q\|_F^2), \quad (14)$$

where $\Theta = \{\Theta^1, \Theta^2, \dots, \Theta^K\}$ is the network parameter to be trained, γ is the regularization parameter. $\hat{\mathbf{x}}_q^k(\Theta^k)$ denotes the output of k -th block. In the implementation, Adam is selected as the optimizer [46]. Therefore, the optimal parameters Θ are obtained by minimizing the loss function (14) for all training data. For a given undersampled exponential signal $\hat{\mathbf{y}}$ which needs to be reconstructed, we feed it into the trained network and get the reconstructed result $\hat{\mathbf{x}} = f(\hat{\mathbf{y}}, \Theta)$.

Hyper-parameters of DHMF includes the rank r we set when factorizing the Hankel matrix $\mathcal{R}\mathbf{y}_q$ to initial $\mathbf{P} \in \mathbb{C}^{n_1 \times r}$ and $\mathbf{Q} \in \mathbb{C}^{n_2 \times r}$, numbers of blocks for the entire network and layers in each block, kernel size of convolution layers, γ for the regularization term in loss function, learning rate for Adam scheme, and the parameter λ in data consistency module. As for the rank r in LRHMF, an experimental way is to set r about 0.1 times the length of signal. Thus, in this implementation, we set r to 20 for LRHMF and DHMF when the lengths of testing signals are 255. Details about settings of r can be found in Section VI. Finally, considering the balance between training time, memory usage, and recovery quality, we set block number to 5 and layers number to 8 to build our network. We observe that the reconstruction results perform well for all the tested data when setting the kernel size to 3×3 and regularization parameter γ to 10^{-2} . The learning rate starts from 10^{-3} and gradually reduces to $\sqrt{10} \cdot 10^{-6}$ with the decrease of the reconstruction RLNE of validation dataset.

Recently, deep learning has been introduced into NMR spectroscopy to reconstruct undersampled signals [40]. The method stacks several dense convolution neural networks together and intermediately reconstructed spectra are further refined by data consistency. Thus, the spectrum artifacts are

TABLE I: Parameters for 1D synthetic exponential signal

Parameters	Number of exponentials(J)	Amplitude (A)	Normalized frequency(f)	Damping factor(τ)	Phase (ϕ)
Minimum	1	0.05	0	10	0
Increment	1	6.9e-18~ 2.22e-16	1.73e-18~ 1.11e-16	1.78e-15~ 2.84e-14	4.90e324~ 8.8e-16
Maximum	10	1	1	179.2	2π

Note: The number of peaks increase from 1 to 10 and length of signal is 255, each subset contains a specific number of peaks and other parameters are acquired uniformly at random using Matlab. Thus, we have 10 subsets and each of them consists 4000 signals. The increment is acquired by calculation the accuracy of the float numbers.

gradually removed in frequency domain through the dataflow of the network. We call it dense convolution neural network (DCNN) throughout the paper.

To exhibit the performance of DHMF on both synthetic data and realistic NMR data, the proposed method will be compared with three state-of-the-art approaches, including low-rank Hankel matrix (LRHM) [7], low-rank Hankel matrix factorization (LRHMF) [11], and dense convolutional neural network (DCNN) [40]. It is worth mentioning that the parameter λ has the same meaning in all methods. For noise-free synthetic data, we set λ to 10^6 . While for noisy synthetic data and realistic data, we set λ to $\sqrt{10}$ in DHMF, 10^3 in DCNN, and $\sqrt{10} \times 10^2$ in both LRHM and LRHMF, if not specified. Details about settings of λ can be found in Section VI.

V. RESULTS

In this section, we evaluate the performance of the proposed DHMF from different perspectives. We first introduce the way we generate datasets and train the network. Then we compare the performance of DHMF on both synthetic data and realistic NMR data with three state-of-the-art approaches. It is worth noting that the DHMF method we use is the enhanced DHMF.

In this implement, all experiments were carried out in a computer server equipped with one Intel i9 9900X CPU (3.5 GHz, ten cores), 128 GB RAM, and three Nvidia RTX 2080Ti GPU card. The proposed DHMF and DCNN networks were implemented in python 3.6, using the Keras 2.2.4 package and Tensorflow 1.14.0 as backend [], and trained using one Nvidia RTX 2080Ti GPU card. The LRHM and LRHMF was coded in MATLAB (Mathworks Inc.) and ran with ten cores, which was parallelized to reduce the computation time under multiple CPU cores maximally.

A. Synthetic data

1) Generating datasets and training

DHMF is trained using backpropagation in supervise manner. We first generate synthetic fully sampled time-domain exponential signals s in the form of (1), undersampling operator U , and their corresponding undersampled signal y formed by $y = Us$. Let q denote the q -th sampling trial, then multiple pairs of $(y_q, s_q, U_q)(q = 1, 2, \dots, Q)$ are formed and used for network training. Meanwhile, we denote \hat{x}_q as the final

reconstructed signal, \hat{P}_q and \hat{Q}_q as the output of P and Q updating module.

After initializing the network as the description in network structure, we then apply data pairs $(y_q, s_q, U_q)(q = 1, 2, \dots, Q)$ to our network. With undersampled data y_q being the initial value for variable x in the first block, we sequentially update matrix P , Q and D . Finally, all these updated variables are imported into the data consistency module and the restored signal of the first block is achieved as the output. Thus, \hat{x}_q shall be the output of data consistency module in the last block. Let the superscript number $k(k = 1, 2, \dots, K)$ denotes the k -th reconstruction block, we have $\hat{x}_q = \hat{x}_q^K$.

In this implement, the proposed network is solely trained by synthetic data. The fully sampled time-domain exponential signal is in the form of (1) whose parameter is shown as TABLE I. Thus, we generate the ground truth data $y = [y_1, \dots, y_{255}]^T$, where $y_n = \sum_{j=1}^J A_j e^{(2\pi i f_j - 1/\tau_j)n + i\phi_j} + \delta, n = 0, \dots, 254$. δ denotes noise which meets Gaussian distribution with a level of $5e-2$. The undersampling operator U follows the Poisson-gap sampling scheme [13]. We then simulate $Q = 40000$ pairs. In each training stage, the dataset was split into 90%/10% for training and validation, respectively.

2) Reconstruction results

We then conduct a series of experiments to exhibit the reconstruction performance of the proposed method. In this implement, exponential signals for reconstruction are generated in the form of (1), and Gaussian noise with the level of $5e-2$ is added. The length of them are 255, and their parameters are randomly selected from TABLE I. To obtain different undersampled signals, we then utilize Poisson-gap sampling scheme with several sets of sampling ratio (SR). For each (J, SR) pair, 100 Monte Carlo trials are conducted to examine the reconstruction errors for accurate recovery.

Fig.4 is the reconstruction errors of synthetic exponential signals from the four compared methods. It shows that DHMF yields a smaller average RLNE than LRHM, LRHMF, and DCNN, when SR is over 15% and the number of exponentials is less than 6. For each method, we draw out the bound where

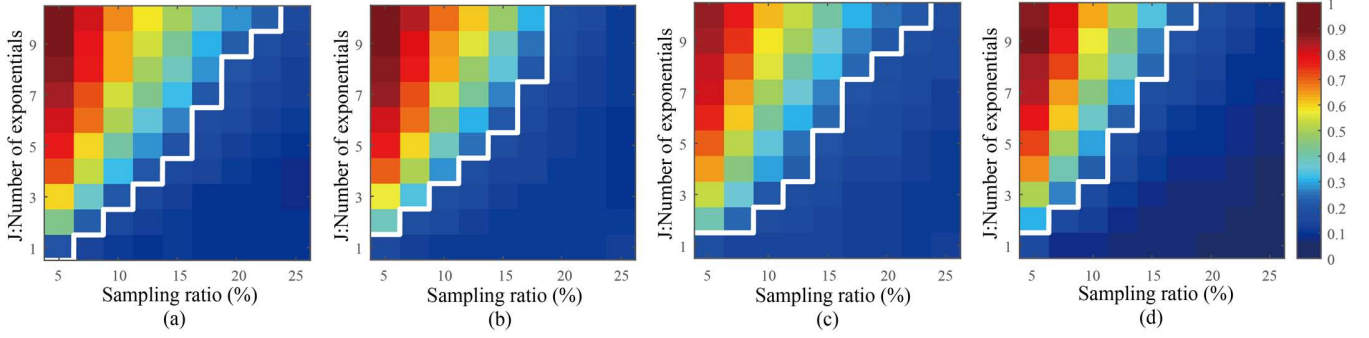


Fig. 4. Reconstruction errors from LRHM, LRHMF, DCNN, and DHMF approaches. (a), (b), (c), and (d) reflect the average RLNEs for recovering undersampled complex exponential signals over 100 Monte Carlo trials by LRHM, LRHMF, DCNN, and DHMF, respectively.

TABLE II: Average score of parameter estimation errors from LRHM, LRHMF, DCNN, and DHMF

Method	Average score			
	Frequency	Amplitude	Damping factor	Phase
LR	2.50	2.49	1.94	2.54
LRHMF	2.60	2.54	2.45	2.55
DCNN	2.31	2.26	2.63	2.29
DHMF	2.59	2.71	2.98	2.62

Note: Parameter estimation is performed every time we reconstruct the test signal. For a particular parameter, we provide a score for each method to indicate the performance of its parameter estimation, which is evaluated by the absolute error between the ground truth and the reconstruction parameter. We provide the method with a score 4 if it gets the best performance, while provide with a score 3, 2 and 1 if the method takes the second, third and last place. The average score is based on the average absolute error over 9000 randomly generated test signals.

the reconstruction errors are lower and higher than 0.2 on both sides. It can be observed that the boundary of DHMF is significantly shifted to low SR and high exponential numbers than that of LRHM and DCNN, and is slightly shifted than LRHMF when the exponential number ranges from 5 to 9. It means that, DHMF requires less sampled entries than LRHM, LRHMF, and DCNN for a stable recovery around the boundary. When SR reduces below 10% and the exponential number is more than 4, reconstruction errors of DCNN and DHMF are similar, but lower than LRHM and LRHMF. It is worth mentioning that, LRHMF yields lower RLNE when the exponential number increases under 25% SR because the exponential number is getting closer to rank r we set, which provides a more accurate prior knowledge. We also show the values of reconstruction errors in APPENDIX TABLE I, II, III, IV for more detailed comparison.

We then use these trials for parameter estimation on reconstructed results. Parameters of the ground truth and the reconstructed signal, including frequencies, amplitudes, damping factors and phases, are estimated by ESPRIT [47, 48]. Then we provide a score for each method to indicate the absolute error between the ground truth and the reconstruction parameter using different methods (TABLE II).

TABLE II illustrates that DHMF possesses the highest average score of parameter estimation errors in terms of amplitudes, damping factors and phases. And is comparable to LRHMF in the estimation of frequencies. These results imply that, DHMF presents more faithful parameter estimations than other state-of-the-art methods. We also show the reconstructed

parameter estimation on one of these random trails (APPENDIX Fig.1), whose parameter is shown in APPENDIX TABLE V, for detail comparison.

We further test the reconstruction ability of DHMF on weak peaks. The frequency domain of the exponential signal is shown as Fig. 5(a), while its detailed parameters are listed in

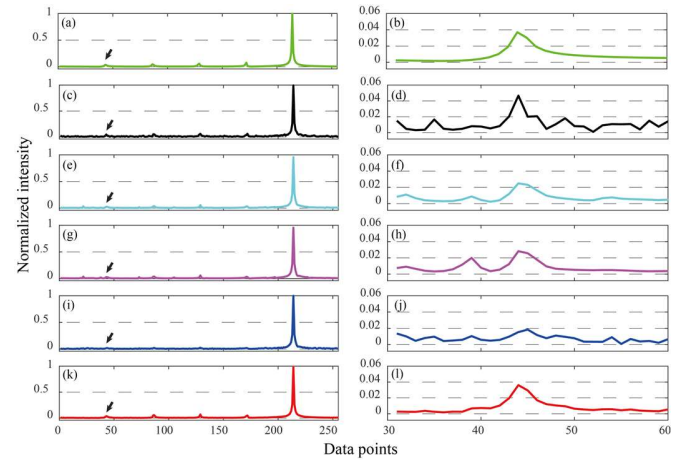


Fig. 5. Reconstructed synthetic signals with weak peaks in frequency domain from 25% NUS data. (a) is the fully sampled noise-free reference signal. (c) is the test data with the Gaussian noise level $\delta=0.05$, (e), (g), (i), and (k) are the reconstructed test data of LRHM, LRHMF, DCNN, and DHMF. (b), (d), (j), (h), and (f) are the zoomed out weak peaks indicated by the arrow.

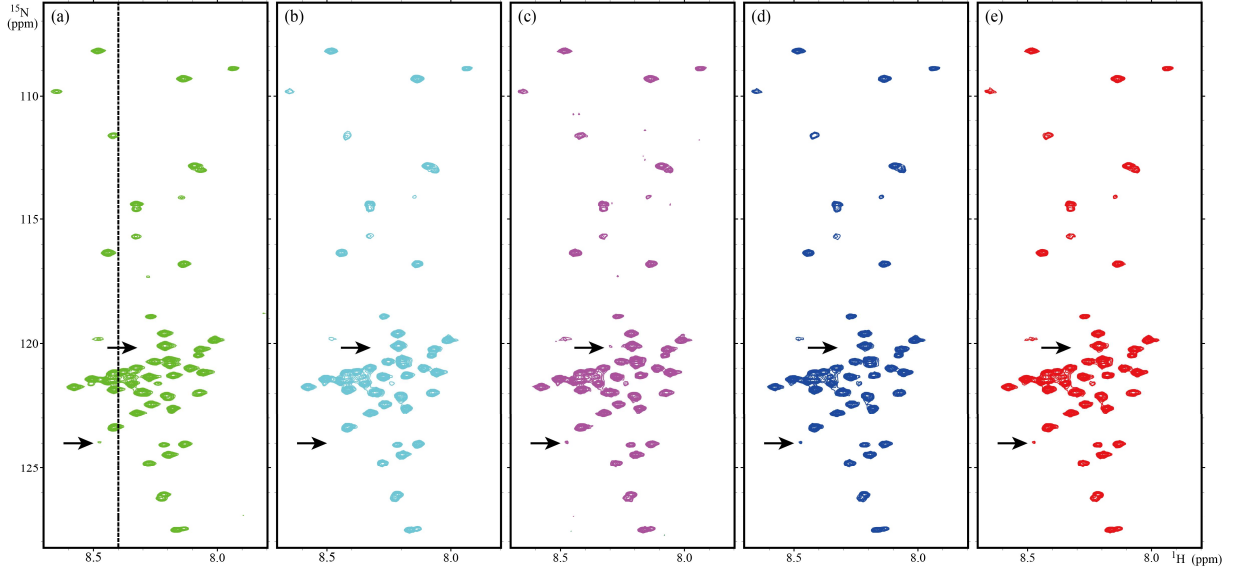


Fig. 6 The NMR spectrum recovery from 25% NUS data. (a) is the referenced fully sampled NMR spectrum. (b), (c), (d), and (e) are the reconstructed results from LRHM, LRHMF, DCNN, and DHMF, respectively. The ppm denotes parts per million by frequency, which is the unit of chemical shift. The NUS spectrum is additionally added noise with the level of $1e-2$. Note that regularization parameter λ and rank r in LRHMF are set to 10^2 and 10, respectively.

APPENDIX TABLE VI. Gaussian noise with the level of $5e-2$ is also added.

Fig. 5 shows that DHMF can faithfully reconstruct weak peaks with more accurate shapes. It is also observed that DCNN can hardly retrieve weak peaks, while LRHM and LRHMF may introduce pseudo peaks and weaken the weak peaks. Average RLNE of LRHM, LRHMF, and DCNN over 100 resampling trials are 0.0933, 0.1021 and 0.1371, respectively, while that of DHMF is only 0.0591.

B. Realistic NMR data

NMR spectroscopy is one of the most powerful tools for the analysis of the composition and structure of various organic and inorganic substances. In NMR experiments, we get NMR time-domain signals, which can be considered as a superposition of damped exponential functions, from machine, and take the Fourier transform to get the spectrums. NUS approach is commonly used to reduce the number of measurements due to the expensive time cost [7], [13-18], where only a small fraction NMR signals are performed and, therefore, only a fraction of measurement time is spent. This motivate the pursuit of reconstructing high-quality NMR spectrum from NUS data.

LRHM, LRHMF, and DCNN have been proved effective and are highly praised by the industry in NMR spectrum reconstruction [7], [11], [40]. In this section, a ^1H - ^{15}N spectrum undersampled by Poisson-gap sampling scheme is used for reconstruction. The spectrum is composed by a matrix with the size of 255×116 , where its columns and rows represent ^1H and ^{15}N dimensions, respectively. According to the principle of the NMR experiment, the undersampling is only performed on rows and each undersampled column can be reconstructed individually.

The reconstructed spectra using the 25% sampling rate are

plotted in Fig. 6, indicating that DHMF leads to a faithful recovery. The marked arrows in Fig. 6 shows that LRHM may severely underestimate some peaks, while LRHMF introduce artifacts. It seems that DCNN performs similar as DHMF. Therefore, we further present comparison on one ^{15}N trace of the reconstructed spectra and peak intensity correlation. Fig. 7 shows that DHMF achieves a faithful recovery, while LRHM weakens many peaks like the marked one (Fig. 7(b)), LRHMF introduces many pseudo peaks, and DCNN remains much noise which leads to baseline oscillation.

Fig. 8 shows the comparison of peak intensity correlation. It is observed that DHMF achieves the highest R^2 among all the four methods, indicating that DHMF can achieve higher

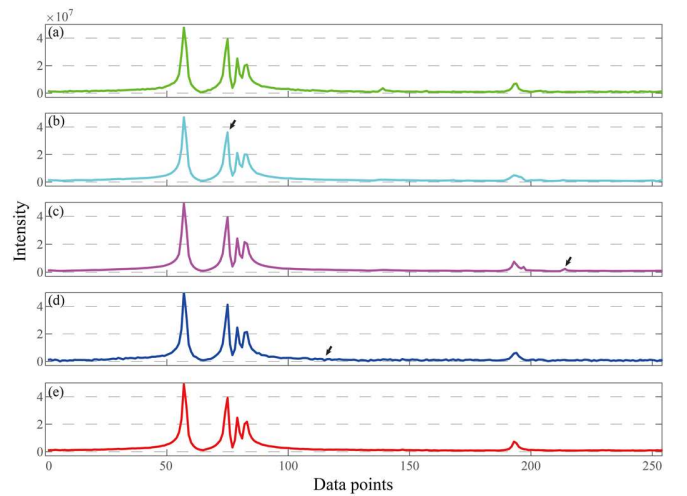


Fig. 7. One trace of the reconstructed spectra. The spectrums are selected along the dimension of ^{15}N and is located at 8.06 ppm on the dimension of ^1H (black line in the Fig. 6).

accuracy of peak intensities during the reconstruction of realistic NMR spectra.

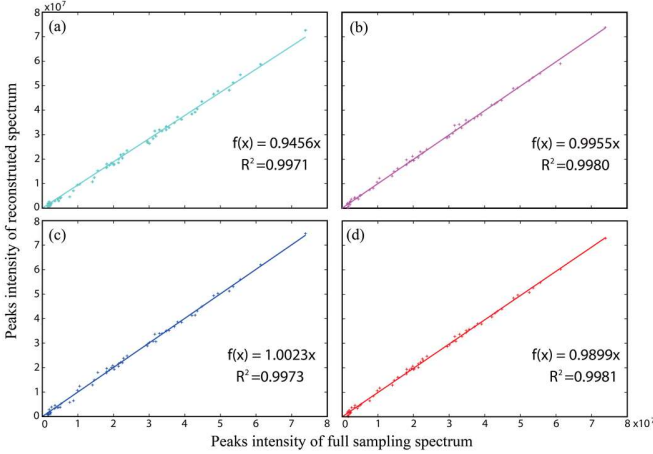


Fig. 8. Peak intensities correlation between the fully sampled spectrum and the reconstructed spectrum. (a), (b), (c), and (d) are correlation evaluation for LRHM, LRHMF, DCNN, and DHMF. R^2 denotes the Pearson's linear correlation coefficient of fitted curve. The closer the value of R^2 is to 1, the stronger the correlation between the reconstructed spectrum and the fully sampled spectrum is.

VI. DISCUSSION

A. Parameter setting

Parameters need to be discussed include regularization parameter λ in all the four methods and rank r in LRHMF and DHMF. Regularization parameter λ is used to balance between the acquired data points in the initial data and the predicted data points. For λ in LRHM and LRHMF, a too large λ may introduce noise while a too small λ tends to smoothen peaks [11], which means choosing a proper regularization

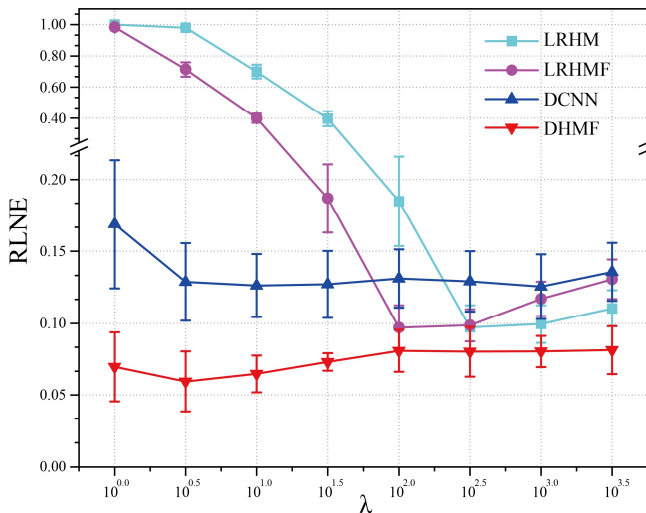


Fig. 9. Average RLNE over 100 NUS resampling trials under different λ . Detail parameters of the testing synthetic signal are shown as APPENDIX TABLE VII. The error bars are the standard deviations of the RLNE. The sampling ratio $SR=25\%$.

parameter is very important for the iterative methods.

Here, we conduct an experiment in which the undersampled test data is the same as APPENDIX TABLE VII to exhibit the influence of the change of λ on different methods. For DCNN and DHMF, training datasets are the same as that in section V, while the only variable for all approaches is λ . Fig. 9 implies that, compared with LRHM, LRHMF, and DCNN, DHMF is less sensitive to the change of λ than the former two methods, and can achieve lower reconstructed errors under the same λ than the latter one.

It is worth mentioning that LRHMF achieves lower RLNE when rank r is set to equal to the number of peaks in undersampled signals. Thus, for synthetic testing signal we already know, we can set r equal to the number of peaks to achieve better performance. Fig. 10(a) shows that LRHMF yields lower RLNEs when getting the optimal r . However, it is impossible to optimize the value of r in practice since we do not know the number of exponentials. And when the number of dimensions of the signal is more than one, it's unpractical to set an optimal r because the exponential number on each slice is different from each other. Fig. 10(b) shows that the proposed DHMF possesses the similar reconstruction errors when adjusting r to 10, indicating that our method is less sensitive to the parameter r than LRHMF.

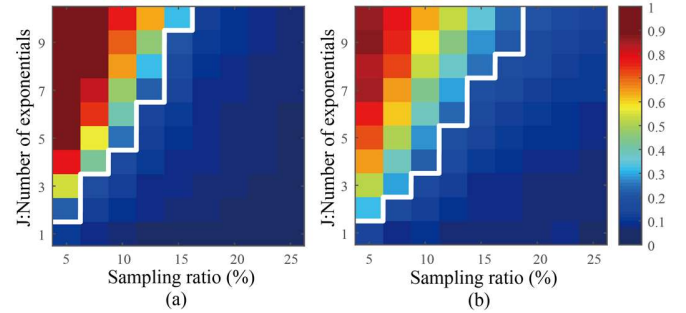


Fig. 10. Reconstruction errors of LRHMF with an optimal rank r and DHMF with rank $r=10$. (a) and (b), reflect the average RLNEs over 100 Monte Carlo trials by LRHMF and DHMF, respectively, in recovering undersampled complex exponential signals.

B. Computational time for reconstructions

One of the advantages of DL is that it can accelerate the reconstruction process by utilizing massive parallel computing of graphic processing units (GPUs) through low complexity neural network algorithms. Though the training stage of network is time-consuming, this process only needs to be performed once. For a trained network, its reconstruction process is much faster than traditional iterative methods.

Comparison of computational time on synthetic data with different sizes is shown in TABLE III. Indicating that DHMF approach is slower than DCNN due to higher network complexity. While compared with the iteration methods LRHM and LRHMF, DHMF cost a similar computational time under the size 255×1 , and is significantly getting faster than other two methods with the increase of the signal size.

TABLE III: Computational time on exponential signals with different sizes (Unit: second)

method \ size	255×1	511×1	1023×1	2047×1
LRHM	1.3251	5.0492	40.1324	664.001
LRHMF	1.0334	8.5586	44.3449	205.4486
DCNN	0.0252	0.0378	0.0627	0.1218
DHMF	1.2435	3.9911	15.0627	63.2354

VII. CONCLUSION

In this work, we propose a new network structure, called DHMF, for the complex exponential signal recovery. Experimental results on the noisy synthetic data demonstrate that, compared with state-of-the-art methods, LRHM, LRHMF, and DCNN, DHMF is in pair with or, mostly, surpass others in performs of reconstructed errors and parameter estimation, while is faster and less sensitive to parameters than iterative methods. It is also empirically observed that DHMF can reconstruct weak peaks more accurately than LRHM, LRHMF, and DCNN. Further experiments on reconstruction of NUS NMR spectrum also imply that, DHMF may effectively promote the development of NMR spectroscopy in chemistry and biology, due to its faithful recovery and high-speed.

VIII. ACKNOWLEDGMENTS

The authors would like to thank V. Orekhov and M. Mayzel for sharing the NMR data.

REFERENCES

- [1] A. Hirose and S. Yoshida, "Generalization characteristics of complex-valued feedforward neural networks in relation to signal coherence," *IEEE Transactions on Neural Networks and Learning Systems*, vol. 23, no. 4, pp. 541-551, 2012.
- [2] D. Nion and N. D. Sidiropoulos, "Tensor algebra and multidimensional harmonic retrieval in signal processing for MIMO radar," *IEEE Transactions on Signal Processing*, vol. 58, no. 11, pp. 5693-5705, 2010.
- [3] C. Qian, L. Huang, M. Cao, J. Xie, and H. C. So, "PUMA: An improved realization of MODE for DOA estimation," *IEEE Transactions on Aerospace and Electronic Systems*, vol. 53, no. 5, pp. 2128-2139, 2017.
- [4] L. Schermelleh, R. Heintzmann, and H. Leonhardt, "A guide to super-resolution fluorescence microscopy," *Journal of Cell Biology*, vol. 190, no. 2, pp. 165-175, 2010.
- [5] J. A. Tropp, J. N. Laska, M. F. Duarte, J. K. Romberg, and R. G. Baraniuk, "Beyond Nyquist: Efficient sampling of sparse bandlimited signals," *IEEE Transactions on Information Theory*, vol. 56, no. 1, pp. 520-544, 2010.
- [6] M. Vetterli, P. Marziliano, and T. Blu, "Sampling signals with finite rate of innovation," *IEEE Transactions on Signal Processing*, vol. 50, no. 6, pp. 1417-1428, 2002.
- [7] X. Qu, M. Mayzel, J. F. Cai, Z. Chen, and V. Orekhov, "Accelerated NMR spectroscopy with low-rank reconstruction," *Angewandte Chemie International Edition*, vol. 54, no. 3, pp. 852-854, 2015.
- [8] H. M. Nguyen, X. Peng, M. N. Do, and Z.-P. Liang, "Denoising MR spectroscopic imaging data with low-rank approximations," *IEEE Transactions on Biomedical Engineering*, vol. 60, no. 1, pp. 78-89, 2012.
- [9] H. Lu, X. Zhang, T. Qiu, J. Yang, D. Guo, Z. Chen, and X. Qu, "Low rank enhanced matrix recovery of hybrid time and frequency data in fast magnetic resonance spectroscopy," *IEEE Transactions on Biomedical Engineering*, vol. 65, no. 4, pp. 809-820, 2017.
- [10] J. Ying, H. Lu, Q. Wei, J. Cai, D. Guo, J. Wu, Z. Chen, and X. Qu, "Hankel matrix nuclear norm regularized tensor completion for n-dimensional exponential signals," *IEEE Transactions on Signal Processing*, vol. 65, no. 14, pp. 3702-3717, 2017.
- [11] D. Guo, H. Lu, and X. Qu, "A fast low rank Hankel matrix factorization reconstruction method for non-uniformly sampled magnetic resonance spectroscopy," *IEEE Access*, vol. 5, pp. 16033-16039, 2017.
- [12] S. Ye, E. Aboutanios, D. S. Thomas, and J. M. Hook, "Localised high resolution spectral estimator for resolving superimposed peaks in NMR signals," *Signal Processing*, vol. 130, pp. 343-354, 2017.
- [13] S. G. Hyberts, K. Takeuchi, and G. Wagner, "Poisson-gap sampling and forward maximum entropy reconstruction for enhancing the resolution and sensitivity of protein NMR data," *Journal of the American Chemical Society*, vol. 132, no. 7, pp. 2145-2147, 2010.
- [14] V. Y. Orekhov and V. A. Jaravine, "Analysis of non-uniformly sampled spectra with multi-dimensional decomposition," *Progress in Nuclear Magnetic Resonance Spectroscopy*, vol. 59, no. 3, pp. 271-292, 2011.
- [15] X. Qu, X. Cao, D. Guo, and Z. Chen, "Compressed sensing for sparse magnetic resonance spectroscopy," in *International Society for Magnetic Resonance in Medicine 18th Scientific Meeting*, 2010, vol. 10, p. 3371.
- [16] K. Kazmierczuk and V. Y. Orekhov, "Accelerated NMR spectroscopy by using compressed sensing," *Angewandte Chemie International Edition*, vol. 50, no. 24, pp. 5556-5559, 2011.
- [17] D. J. Holland, M. J. Bostock, L. F. Gladden, and D. Nietlispach, "Fast multidimensional NMR spectroscopy using compressed sensing," *Angewandte Chemie International Edition*, vol. 50, no. 29, pp. 6548-6551, 2011.
- [18] X. Qu, D. Guo, X. Cao, S. Cai, and Z. Chen, "Reconstruction of self-sparse 2D NMR spectra from undersampled data in the indirect dimension," *Sensors*, vol. 11, no. 9, pp. 8888-8909, 2011.
- [19] E. J. Candès, J. Romberg, and T. Tao, "Robust uncertainty principles: Exact signal reconstruction from highly incomplete frequency information," *IEEE Transactions on Information Theory*, vol. 52, no. 2, pp. 489-509, 2006.
- [20] V. Chandrasekaran, B. Recht, P. A. Parrilo, and A. S. Willsky, "The convex geometry of linear inverse problems," *Foundations of Computational Mathematics*, vol. 12, no. 6, pp. 805-849, 2012.
- [21] J. Ying, F. Delaglio, D. A. Torchia, and A. Bax, "Sparse multidimensional iterative lineshape-enhanced (SMILE) reconstruction of both non-uniformly sampled and conventional NMR data," *Journal of Biomolecular NMR*, vol. 68, no. 2, pp. 101-118, 2017.
- [22] V. Jaravine, I. Ibraghimov, and V. Y. Orekhov, "Removal of a time barrier for high-resolution multidimensional NMR spectroscopy," *Nature Methods*, vol. 3, no. 8, p. 605, 2006.
- [23] M. Fazel, T. K. Pong, D. Sun, and P. Tseng, "Hankel matrix rank minimization with applications to system identification and realization," *SIAM Journal on Matrix Analysis and Applications*, vol. 34, no. 3, pp. 946-977, 2013.
- [24] I. Markovsky and K. Usevich, "Structured low-rank approximation with missing data," *SIAM Journal on Matrix Analysis and Applications*, vol. 34, no. 2, pp. 814-830, 2013.
- [25] Y. Chen and Y. Chi, "Robust spectral compressed sensing via structured matrix completion," *IEEE Transactions on Information Theory*, vol. 60, no. 10, pp. 6576-6601, 2014.
- [26] J.-F. Cai, X. Qu, W. Xu, and G.-B. Ye, "Robust recovery of complex exponential signals from random Gaussian projections via low rank Hankel matrix reconstruction," *Applied and Computational Harmonic Analysis*, vol. 41, no. 2, pp. 470-490, 2016.
- [27] K. Usevich and P. Comon, "Hankel low-rank matrix completion: Performance of the nuclear norm relaxation," *IEEE Journal of Selected Topics in Signal Processing*, vol. 10, no. 4, pp. 637-646, 2016.
- [28] I. Markovsky, "Recent progress on variable projection methods for structured low-rank approximation," *Signal Processing*, vol. 96, pp. 406-419, 2014.

- [29] X. Peng, C. Lu, Z. Yi, and H. Tang, "Connections between nuclear-norm and Frobenius-norm-based representations," *IEEE Transactions on Neural Networks and Learning Systems*, vol. 29, no. 1, pp. 218-224, 2018.
- [30] J.-F. Cai, E. J. Candès, and Z. Shen, "A singular value thresholding algorithm for matrix completion," *SIAM Journal on Optimization*, vol. 20, no. 4, pp. 1956-1982, 2010.
- [31] K. H. Jin, D. Lee, and J. C. Ye, "A general framework for compressed sensing and parallel MRI using Annihilating filter based low-rank Hankel matrix," *IEEE Transactions on Computational Imaging*, vol. 2, no. 4, pp. 480-495, 2016.
- [32] M. D. Desai and W. K. Jenkins, "Convolution backprojection image reconstruction for spotlight mode synthetic aperture radar," *IEEE Transactions on Image Processing*, vol. 1, no. 4, pp. 505-517, 1992.
- [33] Z. Tian and V. Lottici, "Low-complexity ML timing acquisition for UWB communications in dense multipath channels," *IEEE Transactions on Wireless Communications*, vol. 4, no. 6, pp. 3031-3038, 2005.
- [34] Q. Huang, L. Qu, B. Wu, and G. Fang, "UWB through-wall imaging based on compressive sensing," *IEEE Transactions on Geoscience and Remote Sensing*, vol. 48, no. 3, pp. 1408-1415, 2009.
- [35] J. Ying, J.-F. Cai, D. Guo, G. Tang, Z. Chen, and X. Qu, "Vandermonde factorization of Hankel matrix for complex exponential signal recovery—application in fast NMR spectroscopy," *IEEE Transactions on Signal Processing*, vol. 66, no. 21, pp. 5520-5533, 2018.
- [36] D. Chen, Z. Wang, D. Guo, V. Orekhov, and X. Qu, "Review and prospect: Deep learning in nuclear magnetic resonance spectroscopy," *Chemistry-A European Journal*, DOI: 10.1002/chem.202000246, 2020.
- [37] Y. LeCun, Y. Bengio, and G. Hinton, "Deep learning," *Nature*, vol. 521, no. 7553, pp. 436-444, 2015.
- [38] S. G. Worswick, J. A. Spencer, G. Jeschke, and I. Kuprov, "Deep neural network processing of DEER data," *Science Advances*, vol. 4, no. 8, p. eaat5218, 2018.
- [39] R. Liu, Z. Jiang, X. Fan, and Z. Luo, "Knowledge-driven deep unrolling for robust image layer separation," *IEEE Transactions on Neural Networks and Learning Systems*, vol. 31, no. 5, pp. 1653-1666, 2020.
- [40] X. Qu, Y. Huang, H. Lu, T. Qiu, D. Guo, A. Tatiana, O. Vladislav, Z. Chen "Accelerated nuclear magnetic resonance spectroscopy with deep learning," *Angewandte Chemie International Edition*, vol. 59, no. 26, pp. 10297-10300, 2020.
- [41] N. Srebro, *Learning with matrix factorizations*. 2004.
- [42] M. Signoretto, V. Cevher, and J. A. K. Suykens, "An SVD-free approach to a class of structured low rank matrix optimization problems with application to system identification," *Organometallics*, vol. 12, pp.4283-4285, 2013
- [43] S. Tomov, R. Nath, P. Du, and J. Dongarra, "MAGMA users' guide," 2011.
- [44] G. Huang, Z. Liu, L. Van Der Maaten, and K. Q. Weinberger, "Densely connected convolutional networks," in *Proceedings of the IEEE Conference on Computer Vision and Pattern Recognition*, pp. 4700-4708, 2017.
- [45] W. Lee, M. Tonelli, and J. L. Markley, "NMRFAM-SPARKY: Enhanced software for biomolecular NMR spectroscopy," *Bioinformatics*, vol. 31, no. 8, pp. 1325-1327, 2015.
- [46] D. P. Kingma and J. Ba, "Adam: A method for stochastic optimization," *arXiv preprint, arXiv: 1412.6980*, 2014.
- [47] R. Roy and T. Kailath, "ESPRIT-estimation of signal parameters via rotational invariance techniques," *IEEE Transactions on Acoustics, Speech, and Signal Processing*, vol. 37, no. 7, pp. 984-995, 1989.
- [48] P. Stoica and R. L. Moses, "Spectral analysis of signals," 2005.

APPENDIX

A. Parameter estimation of random synthetic signal

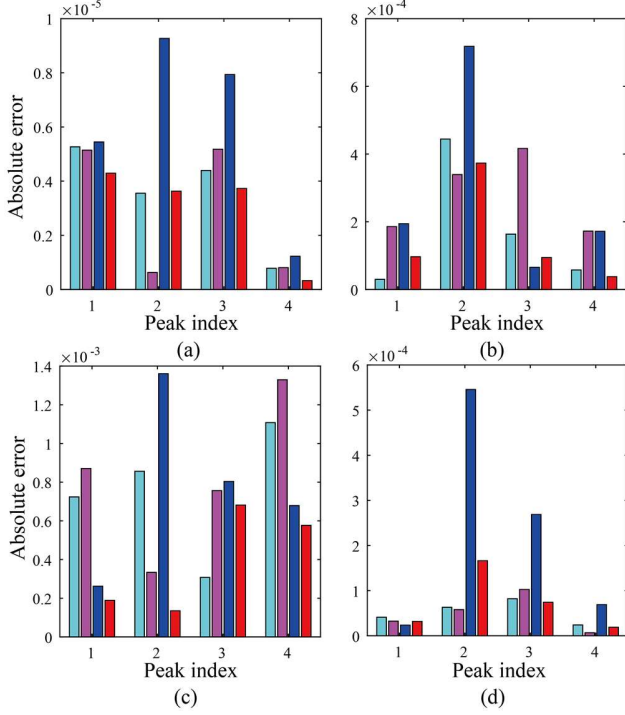


Fig.1 Typical parameter estimation on a random under-sampled signal recovery. Parameters of the signal are listed in TABLE V. (a), (b), (c), and (d) denote parameter estimation of frequency, amplitude, damping factor and phase, respectively. Cyan, purple, blue, and red correspond to the recovery by applying DHMF, DCNN, and LRHMF method, respectively.

B. Detail reconstruction errors

TABLE I: Average reconstruction RLNEs from LRHM

SR J	25%	22.5%	20%	17.5%	15%	12.5%	10%	7.5%	5%
10	0.161	0.220	0.282	0.381	0.482	0.586	0.663	0.809	0.883
9	0.137	0.183	0.228	0.310	0.424	0.540	0.634	0.780	0.887
8	0.123	0.144	0.196	0.272	0.377	0.485	0.631	0.762	0.864
7	0.114	0.130	0.167	0.216	0.312	0.431	0.540	0.712	0.846
6	0.099	0.114	0.140	0.166	0.260	0.343	0.504	0.684	0.801
5	0.093	0.106	0.118	0.146	0.201	0.275	0.411	0.599	0.765
4	0.085	0.094	0.108	0.126	0.150	0.214	0.312	0.533	0.708
3	0.079	0.087	0.088	0.098	0.122	0.151	0.210	0.375	0.595
2	0.085	0.087	0.089	0.097	0.104	0.121	0.156	0.220	0.434
1	0.098	0.092	0.094	0.097	0.100	0.098	0.110	0.133	0.203

TABLE II: Average reconstruction RLNEs from LRHMF

SR J	25%	22.5%	20%	17.5%	15%	12.5%	10%	7.5%	5%
10	0.109	0.141	0.184	0.309	0.476	0.609	0.691	0.833	0.896
9	0.104	0.127	0.165	0.245	0.388	0.554	0.653	0.793	0.904
8	0.102	0.118	0.148	0.207	0.337	0.472	0.635	0.769	0.876
7	0.104	0.112	0.137	0.176	0.260	0.416	0.535	0.718	0.854
6	0.096	0.107	0.121	0.140	0.217	0.301	0.472	0.691	0.802
5	0.096	0.108	0.116	0.135	0.173	0.245	0.376	0.589	0.763
4	0.095	0.101	0.111	0.126	0.135	0.187	0.277	0.504	0.694
3	0.093	0.100	0.101	0.106	0.120	0.140	0.186	0.331	0.565
2	0.102	0.103	0.104	0.108	0.110	0.122	0.145	0.187	0.380
1	0.112	0.104	0.106	0.107	0.108	0.101	0.107	0.115	0.153

TABLE III: Average reconstruction RLNEs from DCNN

SR J	25%	22.5%	20%	17.5%	15%	12.5%	10%	7.5%	5%
10	0.174	0.204	0.253	0.300	0.405	0.528	0.620	0.843	0.853
9	0.151	0.179	0.215	0.268	0.350	0.482	0.579	0.735	0.843
8	0.138	0.152	0.190	0.240	0.317	0.414	0.558	0.701	0.824
7	0.125	0.141	0.173	0.199	0.263	0.362	0.484	0.648	0.808
6	0.113	0.133	0.154	0.165	0.242	0.305	0.424	0.610	0.750
5	0.105	0.124	0.140	0.157	0.197	0.252	0.346	0.519	0.695
4	0.105	0.112	0.130	0.138	0.169	0.221	0.294	0.451	0.648
3	0.103	0.111	0.113	0.121	0.138	0.170	0.216	0.359	0.529
2	0.108	0.109	0.115	0.115	0.128	0.144	0.169	0.231	0.390
1	0.119	0.108	0.118	0.117	0.134	0.125	0.134	0.133	0.190

TABLE IV: Average reconstruction RLNEs from DHMF

SR J	25%	22.5%	20%	17.5%	15%	12.5%	10%	7.5%	5%
10	0.107	0.127	0.189	0.224	0.332	0.504	0.632	0.890	0.874
9	0.093	0.114	0.148	0.196	0.262	0.440	0.573	0.759	0.890
8	0.087	0.096	0.134	0.162	0.233	0.377	0.525	0.722	0.844
7	0.078	0.087	0.116	0.138	0.181	0.285	0.446	0.651	0.836
6	0.067	0.079	0.095	0.104	0.164	0.228	0.366	0.602	0.781
5	0.061	0.076	0.087	0.098	0.120	0.181	0.294	0.491	0.719
4	0.057	0.065	0.076	0.085	0.100	0.140	0.222	0.390	0.659
3	0.050	0.059	0.064	0.070	0.078	0.104	0.150	0.259	0.503
2	0.051	0.053	0.060	0.065	0.070	0.081	0.117	0.146	0.299
1	0.046	0.049	0.058	0.059	0.063	0.065	0.076	0.078	0.138

C. Detail parameters of synthetic signals

TABLE V: Synthetic data with four peaks for APPENDIX Fig.1

Peaks ID Parameters	1	2	3	4
Amplitude (A)	0.100	0.325	0.550	0.775
Damping factor (τ)	50	75	100	125
Phase (ϕ)	$2\pi/5$	$4\pi/5$	$6\pi/5$	$8\pi/5$
Frequency (f)	0.1655	0.3349	0.5004	0.6698

TABLE VI: Synthetic data with five peaks for Fig.5 .

Peaks ID Parameters	1	2	3	4	5
Amplitude (A)	0.100	0.100	0.100	0.100	1.000
Damping factor (τ)	50	75	100	125	150
Phase (ϕ)	$2\pi/5$	$4\pi/5$	$6\pi/5$	$8\pi/5$	2π
Frequency (f)	0.1655	0.3349	0.5004	0.6698	0.8353

TABLE VII: Synthetic data with five peaks for Fig.9.

Peaks ID Parameters	1	2	3	4	5
Amplitude (A)	0.5145	0.6623	0.7253	0.7825	0.9872
Damping factor (τ)	26.47	35.63	48.78	61.51	81.50
Phase (ϕ)	$2\pi/5$	$4\pi/5$	$6\pi/5$	$8\pi/5$	2π
Frequency (f)	0.1532	0.3135	0.4716	0.6124	0.7831